Heliyon 11 (2025) e42568

Contents lists available at ScienceDirect

Heliyon

journal homepage: www.cell.com/heliyon

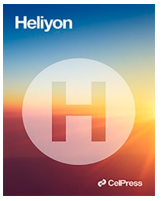

Research article

# Optical vibrational spectroscopic signatures of ammonium diuranate process parameters

Tyler L. Spano [a,*], Caleb Redding [a], Jordan M. Roach [a], Cody A. Nizinski [b], Evan Warzecha [b], Matthew Athon [b], Rodney Hunt [a], Andrew Miskowiec [a], Jennifer Ladd-Lively [a]

[a] Nuclear Nonproliferation Division, Oak Ridge National Laboratory, Oak Ridge, TN, 37831, USA
[b] Pacific Northwest National Laboratory, Richland, WA, 99354, USA

ARTICLE INFO

*Keywords:*
Ammonium diuranate
ADU
Uranyl hydroxide
Uranium ore concentrate
Raman spectroscopy
Nuclear forensics

ABSTRACT

Ammonium diuranate (ADU) is commonly encountered in the nuclear fuel cycle; however, previous investigations have shown that ADU is a complex mixture of distinct compounds. Moreover, production parameters are known to heavily influence the composition of the resulting ADU. Here, we examine four samples of ADU prepared at Oak Ridge National Laboratory (ORNL), and one sample of ADU made at Pacific Northwest National Laboratory (PNNL), with the goal of further characterizing and elucidating the effect of processing parameters such as stir rate, strike direction, and temperature on material composition. Process parameters during ADU precipitation at ORNL and PNNL were well documented, and we relate process variables to optical vibrational spectroscopic signatures observed using Raman and infrared (IR) spectroscopy. In addition, powder X-ray diffraction (PXRD) reveals differences in the solid-phase composition of ADU precipitates, but we find that the primary phase is similar to the uranyl oxyhydroxyhydrate mineral metaschoepite. Despite the significant phase contributions of a metaschoepite-like phase, spectroscopic evidence of both nitrate and ammonium are observed for all samples. To gain a more holistic understanding of spectroscopic features of process parameters in ADU, principal component analysis (PCA) is employed and results in observable signatures that relate to the stir rate used during synthesis. These results provide further information about the process-dependence of ADU precipitate composition.

## 1. Introduction

ADU is ubiquitous in nuclear fuel cycles and is an important intermediate material employed in conversion from uranium ores to uranium oxides. The production of ADU can involve precipitation from uranyl nitrate solutions via addition of gaseous or aqueous ammonia and is followed by conversion to $U_3O_8$ before reduction to uranium dioxide ($UO_2$) for fuel fabrication. Despite well-established process flow sheets that involve ADU, the stoichiometry of this phase is as variable as the production parameters used to prepare it. In fact, recent work highlights inconsistencies in the literature that were first proposed in the middle of the twentieth century [1,2] about the nomenclature and composition of ADU, with the consensus being that ADU is likely a misnomer and that the material is closer to a multiphase mixture of $(UO_3)_3NH_3{\cdot}5H_2O$ and $(UO_3)_2NH_3{\cdot}3H_2O$ [3].

* Corresponding author.
*E-mail address:* spanotl@ornl.gov (T.L. Spano).

https://doi.org/10.1016/j.heliyon.2025.e42568
Received 7 August 2024; Received in revised form 3 February 2025; Accepted 7 February 2025
Available online 12 February 2025

In early investigations of this phase, Cordfunke [4] and Debets and Loopstra [5] delineate several possible solid phases that may result from aqueous equilibrium of $NH_3$–$UO_3$–$H_2O$ and present powder X-ray diffractograms for these. On the other hand, Stuart and Whatley [6] used IR spectroscopy and found no evidence of distinct phases. Cordfunke [1], however, shows the variability present in solid phases precipitated from solutions containing $NH_3$–$UO_3$–$H_2O$—also by IR spectroscopy—and this variability is frequently confirmed in the literature [7]. Hence, the overall consensus seems to indicate that ADU is likely a combination of distinct compounds.

With regard to the morphology of precipitates of ADU, details about the solid-phase morphology related to the precipitation conditions for ADU phases are abundant. The temperature, pH, ammonium concentration, and stir rate [3,8–10] of the solution from which ADU is precipitated using either gaseous or aqueous ammonium hydroxide ($NH_4OH$) are recognized as contributing factors to variability of both crystallite size and morphology of solid-phase products [11]. Likewise, the addition of ammonia to a uranyl solution (forward strike) or uranyl to an ammonia solution (reverse strike) can result in variable reaction products. These influences persist through later stages of solid-phase processing when ADU is converted to uranium oxides [12,13]. Differences in thermal decomposition behavior of ADU are also noted as potential indicators of process history [14]. ADU and uranyl oxyhydroxyhydrate phases have been observed on $UO_2$ during aging studies, again illustrating the variety of formation conditions that can lead to ADU and highlighting the importance of provenance determination for nuclear materials [15]. Thus, correlations between process parameters and physical appearance can be employed to provide insight into process history of materials composed of, or from, ADU.

More recently, Bonales et al. provide an excellent systematic study [16] of the Raman spectroscopic signatures of ADU as a function of preparation conditions. These researchers summarize existing optical vibrational spectroscopic data that appear in the ADU literature [17–21] and provide a detailed analysis of spectra collected for ADU precipitated with various $NH_4OH$ concentrations. Although the work by Bonales et al. provides important insight about the precipitation mechanisms of ADU and some details about solid-phase precipitates as they relate to safe operation of processing facilities, the focus here is on establishing correlations between solid-phase ADU and the processes used to form it as potential indicators of material provenance. Building from the previous investigations of this material—specifically, the identification of multiple solid-phase components of ADU precipitates and the apparent sensitivity of those materials to processing conditions—we employ a combination of optical vibrational spectroscopy and PXRD to correlate crystal phase and spectroscopic properties of ADU precipitates to differences in material preparation parameters. We use the current state of the literature to examine samples of ADU prepared at ORNL and PNNL with varied production parameters. First, we identify the multiphase mixtures that result from various ADU precipitations using PXRD. Then, we compare multiple Raman spectra collected on each sample of ADU to assess sample homogeneity and potential intrasample variability. Raman and IR spectra collected for all samples are then compared and discussed to describe the intersample variability that may originate from process variables. Throughout, we provide Raman spectra for all ADU phases examined in this work in the low-energy (~40–500 $cm^{-1}$) region, which have not been discussed elsewhere in detail to the best of our knowledge. We find that the primary precipitate that results from ADU preparation is similar to the mineral phase metaschoepite, and use Raman assignments proposed by Colmenero et al. to describe potential structural origins of spectroscopic features [22]. IR spectra collected for ADU further reveal differences in solid-phase precipitates that result from variable synthesis procedures. Finally, we use PCA to describe subtle variability in sample spectra as they may relate to variations in processing procedures. By combining multiple spectroscopic techniques with X-ray diffraction, we attempt to elucidate the relationships between the details of the multiphase mixture of ADU precipitates and the production parameters. Moreover, the combination of multiple techniques allows us a holistic view of ADU phase space and permits us to suggest plausible chemical mechanisms that may result in differences between resulting materials based on those production parameters.

## 2. Materials and methods

### 2.1. Synthesis

To explore optical vibrational spectroscopic signatures of ADU and the underlying structural features from which they originate, five samples were synthesized with varying process parameters resulting in solid samples with well-pedigreed history, and they are summarized in Table 1. The first ADU precipitation (ADU1) was performed at PNNL where approximately 400 g of precipitate was prepared in a custom-made vessel with baffles and a draft tube (Fig. S1a, supporting information). The aqueous uranyl nitrate ($UO_2(NO_3)_2$) feed was prepared by dissolving 448 g of $UO_2$ stock (395 g U) by the slow addition of 1.0 L of 7 M nitric acid ($HNO_3$, Fisher Chemical, Optima grade) while stirring, which was done using a ServoDyne mixer; the uranyl nitrate was then diluted with an additional 1.0 L of deionized (DI) water. Before precipitation, the feed was heated to 60 °C, and the stirrer was set to mix at a rate of 400 rpm. Over 23 min, 25 v/v% aqueous $NH_4OH$ (Fisher Chemical, ACS grade) was added through an inlet tube via a peristaltic pump

**Table 1**
Production parameters for ADU precipitations.

| Sample ID | Stir rate (rpm) | Temperature (°C) | Strike | Precipitation method |
|---|---|---|---|---|
| ADU1 | 400 | 60 | Forward | Custom vessel |
| ADU2[a] | 400 | 20 | Forward | Jacketed beaker |
| ADU3 | 400 | 20 | Forward | Jacketed beaker |
| ADU4 | 100–130 | 20 | Forward | Jacketed beaker |
| ADU5 | 600–500 | 20 | Forward | Jacketed beaker |

[a] See text for details regarding experimental differences between ADU2 and ADU3.

until a pH of 7.97 was reached. The slurry was then digested at 55–60 °C for 30 min with a final pH of 8.41. The digested product was recovered via vacuum filtration after washing with DI water. The resulting filter cake, representing a 99 % yield (Fig. S1b) was dried under vacuum at room temperature for approximately 1 week.

The first preparation of ADU at ORNL (ADU2) was done by combining Millipore Sigma 28 v/v% aqueous $NH_4OH$ solution (≥99.99 % trace metals basis) at a rate of 3.3 L/min with sufficient aqueous uranyl nitrate feedstock (preparation described in supporting information) to produce an ADU sample containing 100 g of uranium. The aqueous mixture was stirred at a rate of 400 rpm, at 20 °C, during the precipitation, resulting in a slurry of bright yellow precipitate. Due to external factors, the experiment was paused at a pH of 3, and allowed to age without stirring for 1.5 months. After this time, the experiment continued at the 400 rpm stir rate until the pH reached approximately 8. The ADU precipitate was recovered by vacuum filtration and was washed with DI water. Following filtration, the precipitate (ADU2) was dried overnight at approximately 100 °C. The second precipitation at ORNL (ADU3) was prepared similarly to ADU2 but without external disruptions. The experiment began with the addition of 28 % ammonium hydroxide at a rate of 3.3 L/min to aqueous uranyl nitrate containing 100 g U being stirred at 400 rpm in a custom 1 L jacketed beaker. The reagent was added until a pH of 8 was reached. This occurred over a course of about 70 min. The slurry was then allowed to age for approximately 1 h with the stirrer on. After aging, the slurry was transferred to a vacuum funnel and was washed with DI water multiple times following filtration. Like the previous sample, ADU3 was dried overnight at approximately 100 °C. The plan for the third ORNL precipitation (ADU4) was identical to that for ADU3 apart from the stir rate being reduced to 100 rpm. However, 9 min into the $NH_4OH$ addition, large crystallite aggregates appeared on the surface of the aqueous uranyl nitrate and appeared to hinder mixing. This was addressed real-time by adjusting the stir rate to 130 rpm, at which point mixing efficiency appeared to improve. The reagent was added until a pH of 8 was reached, which took about 64 min. The sample was aged with the stirrer on for 1 h. Note, this synthesis resulted in a thick, chalky suspension of precipitate with a large range of particle sizes observed. The sample was transferred to the vacuum filter over the course of 25 min and was washed several times with DI water. ADU5 was prepared in the same manner as ADU3 and ADU4 but was stirred at 600 rpm initially. Approximately 50 min into the precipitation, the stir bar began to move erratically and induce splatter onto the vessel lid. The stir rate was decreased to 500 rpm, and the reagent was added over a total of 65 min. This precipitate was aged for 1 h while stirring. After 1 h of aging, the stir rate was reduced to 350 rpm, and the slurry was recovered by vacuum filtration. ADU5 was washed several times with DI water and dried overnight at 100 °C.

### 2.2. Characterization

PXRD data were collected for all samples of ADU using a Proto AXRD benchtop diffractometer in Bragg–Brentano configuration. Samples were prepared by lightly grinding approximately 50 mg of ADU with a small quantity of NIST640e silicon Standard Reference Material in a mortar and pestle and transferring the sample/SRM mixture to a zero-background silicon substrate. Samples were illuminated with a Cu–Kα ($\lambda = 1.5406$ Å) X-ray source, and data were collected in the range of 10–70 °2θ, with a step velocity of 1° 2θ/min. Phase identification of powder samples was done using the International Centre for Diffraction Data Powder Diffraction File (PDF) 4+ following zero shift corrections done using the known positions of reflections in NIST640e.

A Renishaw inVia™ micro-Raman spectrometer was used to collect data for all samples of ADU which were prepared by transferring small quantities of sample powder to gunshot residue (GSR) tabs. The instrument was calibrated using an internal Si standard. An excitation wavelength of 785 nm was used to collect spectra in the range of 35–1200 $cm^{-1}$ in combination with a 1200 lines/mm holographic notch diffraction grating resulting in a resolution of approximately 2.5–3.1 $cm^{-1}$. Corresponding power densities for Raman measurements were approximately 100 $W/cm^2$ based upon laser power (10 mW) and spot size (~1 μm). Reported spectra are the sum of 20 accumulations, each with a 10 s exposure time. Three spectra were collected for each ADU material to examine potential variability within each sample, with corresponding sample and subsample images shown in Supporting Information Fig. S2. We first examine intrasample variability in the range of 35–1200 $cm^{-1}$ for each sample as this is the region of the spectra that contains information regarding U coordination environments. Then, we review potential spectroscopic indicators at higher energy (from 1200 to 1800 $cm^{-1}$). Then, to compare signatures that may arise from variables in sample production, we also compare average spectra calculated for each sample and IR spectroscopy results in the discussion section. Average spectra for each sample were fit to Voigt profiles via a Levenberg–Marquardt nonlinear least-squares approach using the Fityk [23] software package for band analysis.

Scanning electron microscopy images were collected using a Zeiss Gemini 460 field emission scanning electron microscope to explore potential morphological differences that may indicate variability in process parameters. Samples were dusted on GSR tabs and were not carbon coated to preserve sample morphology. Backscatter electron images (25 × 18.75 μm) were collected for all samples using an accelerating voltage of 5 kV and 14 pA current following initial surveys to determine particle homogeneity (see Supporting Information, Fig. S3).

Fourier transform infrared spectra were collected using an attenuated total reflectance (ATR) sample environment on a Bruker INVENIO instrument. Microgram samples of each ADU powder were transferred to the diamond lens of the instrument and pressed using the ATR tip. Data were collected in the range of 370–5000 $cm^{-1}$ and background subtracted using spectra collected in the same region both in air and with no sample pressed between the diamond lens and the ATR tip.

## 3. Results

### 3.1. Powder X-ray diffraction

Analysis of PXRD data collected for samples of ADU highlights the variable composition of this material, with diffractograms of

each sample of ADU showing significant phase mixtures. The ADU1 sample is composed primarily of a synthetic analog of the uranyl oxyhydroxyhydrate mineral phase, metaschoepite ($(UO_2)_4O(OH)_6{\cdot}5H_2O$, PDF card no. 04-011-3920) [24]. Minor phase contributions of $NH_3U_2O_6{\cdot}3H_2O$ (ADU III, PDF card no. 00-037-0628) [25], and $4UO_3{\cdot}NH_3{\cdot}7H_2O$ [26] (PDF card no. 00-031-1428) are also present in the ADU1 sample (Supporting Information Fig. S4). Powder diffraction data collected for the ADU2 sample (Fig. S5) show strong phase contributions from metaschoepite and uranyl hydroxide ($UO_2(OH)_2$, PDF card no. 00-028-1415). Minor phases of $(NH_4)_2U_4O_{13}{\cdot}7H_2O$ (PDF card no. 00-013-0059) and ammonium uranyl nitrate hydrate ($(NH_4)_2UO_2(NO_3)_4{\cdot}2H_2O$, PDF card no. 00-045-0434) [27] are also present in ADU2. The diffractogram collected for the ADU3 sample displays significant peak broadening (Fig. S6). Nevertheless, a mixture of $NH_3U_2O_6{\cdot}3H_2O$ (ADU III), metaschoepite, and $(NH_4)_2U_4O_{13}{\cdot}7H_2O$ (PDF card no. 00-013-0059) [28] includes the main phases contributing to this material. ADU4 (Fig. S7) shows broad reflections, similar to those observed for ADU3 with phase contributions from $2UO_3{\cdot}NH_3{\cdot}3H_2O$ (PDF card no. 00-031-1427) [26] and $UO_3{\cdot}NH_3{\cdot}H_2O$ (PDF card no. 00-039-0586) [14], resulting in the observed diffractogram. Like the other samples of ADU prepared at ORNL, ADU5 displays broad reflections (Fig. S8). Phase contributions for ADU5 include metaschoepite, ADU III, $2UO_3{\cdot}NH_3{\cdot}3H_2O$, and $UO_3{\cdot}NH_3{\cdot}H_2O$. The intrinsic complexity of these samples, as evidenced by the multiphase mixtures observed with PXRD unfortunately preclude quantitative analysis (e.g., determining phase fractions, crystallite domain size, Rietveld refinement). However, we use the qualitative results from PXRD throughout the remainder of this manuscript to understand potential structural origins of spectroscopic features we observe using Raman and IR.

### 3.2. *Raman spectroscopy: intrasample variability in the range of 35–1200 cm$^{-1}$*

The Raman spectra of the ADU1 sample appear quite homogenous (Fig. 1a–c). As described in the Materials and Methods section, three spectra were collected from different particles of to examine intrasample variability within the bulk material. Although some variability in intensity is observed, all spectra are dominated by a prominent peak centered at approximately 840 cm$^{-1}$. While detailed assignments are discussed later, peaks in this region, between 700 and 900 cm$^{-1}$ are generally attributable to symmetric stretching of axial U–O (uranyl, U–$O_{yl}$). This feature shows significant asymmetry with up to three low-energy shoulder peaks contributing to observed intensity based on results from peak fitting. Between 45 and 555 cm$^{-1}$, numerous vibrational modes are observed, with results of fitting suggesting that at least 15 peaks are contributing to observed intensity. At high energy, a peak centered at approximately 1063 cm$^{-1}$ is also seen.

Raman spectra collected for ADU2 sample show significantly more variability than ADU1. Like ADU1, however, the most prominent spectral feature is a large peak centered at approximately 840 cm$^{-1}$. Close examination of this peak shows some evidence of a shift in the peak center between datasets collected for ADU2 (Fig. 2b), and all uranyl peaks show the same asymmetry as observed in ADU1, however. In the region of 1030–1080 cm$^{-1}$, additional inconsistency is seen. One spectrum collected for this sample shows two fairly well-resolved peaks, with the higher intensity feature centered at approximately 1063 cm$^{-1}$. The other two datasets collected for ADU2 clearly show a low-energy shoulder approximately 1045 cm$^{-1}$ associated with the main approximately 1063 cm$^{-1}$ peak in this region (Fig. 2c). In the range of approximately 45–555 cm$^{-1}$, no significant variability is present in the spectroscopic features, although

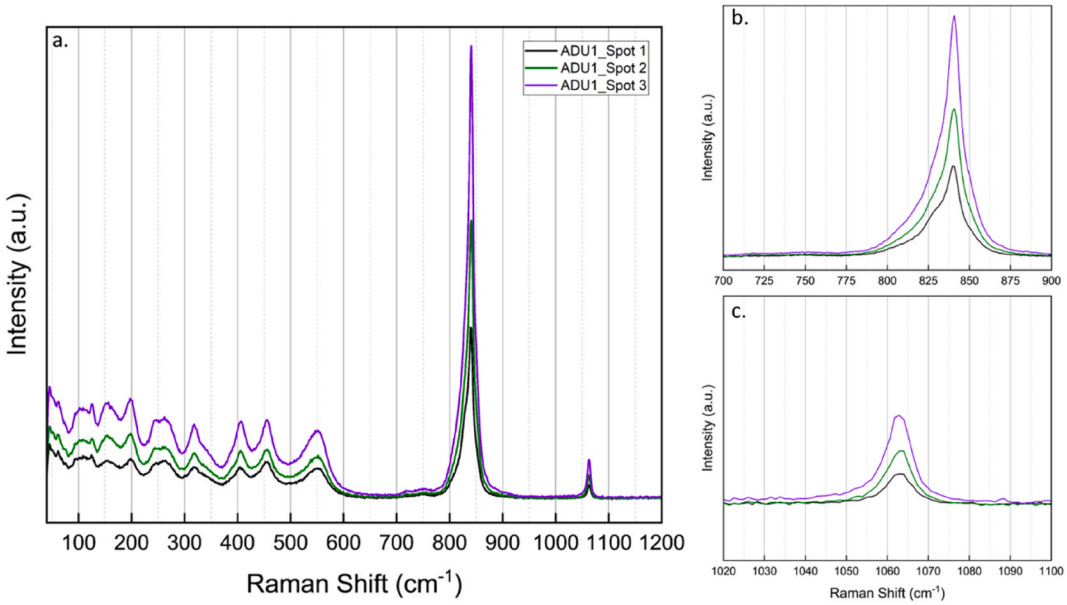


**Fig. 1.** (a) Raman spectra collected for three spots on the ADU1 sample to examine intrasample variability. Limited intrasample variability is observed. (b) The uranyl region of Raman spectra collected for ADU1, showing asymmetry of the $UO_2^{2+}$ symmetric stretching vibrational mode. (c) The high-energy region of the Raman spectra of ADU1.

one dataset appears to have slightly lower resolution of peaks in this spectral range.

Relative to ADU1 and ADU2, the ADU3 sample shows substantial inconsistencies between spectral datasets (Fig. 3). Like ADU2 sample, some variability in resolution of spectral features is visible in the low-energy region (~45–555 $cm^{-1}$) of the spectra (Fig. 3a). Notably, one spectrum shows a distinct difference in the relative intensity of an apparent doublet of peaks between approximately 370 and 485 $cm^{-1}$ when compared to the other two spectra collected for ADU3. A different dataset from ADU3 shows what appears to be a unique feature: a broad apparent doublet between 685 and 780 $cm^{-1}$. Upon closer examination of that same region in the other ADU3 spectra, some contributions from this same feature may be present but with significantly reduced intensity and resolution. Less variability is observed in the U–$O_{yl}$ region, with all spectra displaying a similarly centered peak at approximately 840 $cm^{-1}$, with a lower intensity shoulder at approximately 829 $cm^{-1}$. One of the collected datasets has greater resolution of the low-energy shoulder than we see in other datasets (Fig. 3b). An apparent doublet of modes is present between approximately 1040 and 1075 $cm^{-1}$, with two peaks visible at approximately 1047 and 1063 $cm^{-1}$, albeit with varying relative intensity across the three spectra (Fig. 3c).

Spectra collected for ADU4 are consistent with regard to features in the low-energy region, up to approximately 555 $cm^{-1}$, with some variability in resolution of peaks (Fig. 4). A low-intensity peak is seen in all spectra at approximately 705 $cm^{-1}$ (Fig. 4a). Two (rather than one) low-energy shoulders peak are associated with the main uranyl mode centered at approximately 840 $cm^{-1}$ (Fig. 4b). The apparent peak positions of these shoulder features are approximately 815 and 829 $cm^{-1}$. All spectra collected for ADU4 are consistent in the high-energy region, with a single peak centered at approximately 1047 $cm^{-1}$ (Fig. 4c).

Limited intrasample variability is observed in the spectra of ADU5 (Fig. 5). Consistent spectral features are observed up to approximately 555 $cm^{-1}$, with slight intensity differences across individual datasets. A single spectrum collected for ADU5 has a broad, low-intensity feature centered at approximately 749 $cm^{-1}$ (Fig. 5a). Like we observed in ADU3, this appears to be a low-intensity doublet that is present in all spectra with variable intensity and resolution upon closer examination. All spectra collected for ADU5 show both low- and high-energy shoulders in the uranyl region, with the main peak located at 829 $cm^{-1}$, a low-energy shoulder at approximately 800 $cm^{-1}$, and the high-energy shoulder at approximately 840 $cm^{-1}$ (Fig. 5b). All ADU5 datasets have a single feature at higher energy, with a low-intensity peak observed at approximately 1063 $cm^{-1}$ (Fig. 5c).

### 3.3. *Raman spectroscopy: intrasample variability in the range of 1200–1800 $cm^{-1}$*

In addition to the Raman spectra discussed previously, we also collected data at an extended range to examine the possibility of $NH_4$ vibrational mode contributions (Fig. 6). Assignments for the modes discussed here will be detailed in the next section and in Table 2, however, we outline variability among spectra collected for individual samples to further examine the degree of homogeneity within each ADU material.

Despite the consistent features seen in the ADU1 sample previously, significant variability is observed in the high-energy region. One spectrum shows two broad features centered at approximately 1310 and 1605 $cm^{-1}$. The remaining spectra collected for ADU1 show only very low-intensity features between approximately 1350 and 1520 $cm^{-1}$. Observations for the high-energy spectra of ADU2 are surprisingly quite consistent, given the spectroscopic differences observed in the low-energy region. These datasets are

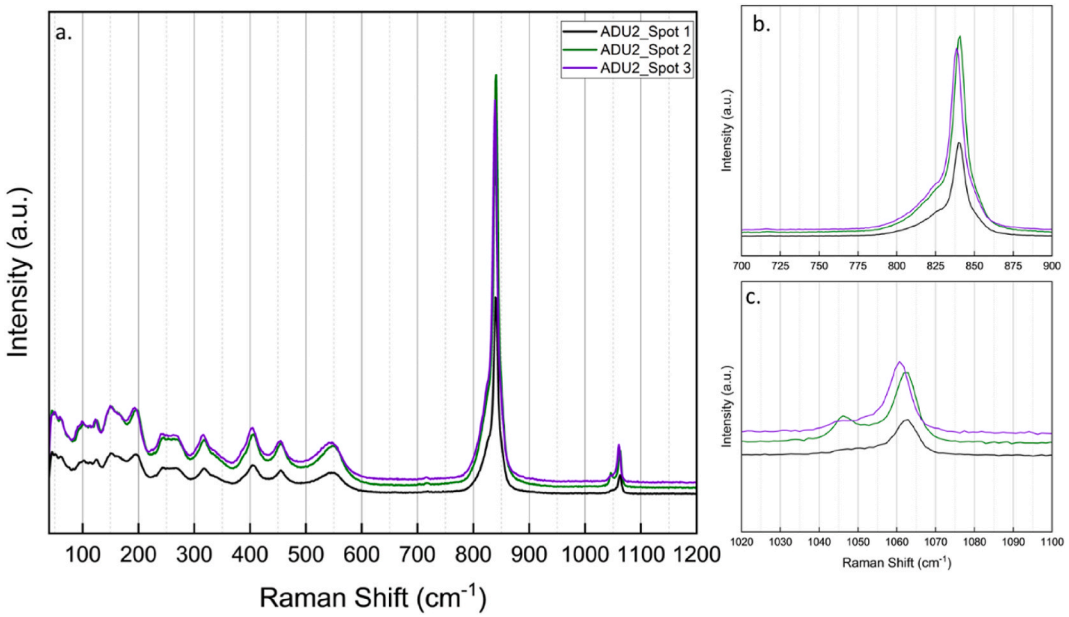


**Fig. 2.** (a) Raman spectra collected for three spots on the ADU2 sample to examine intrasample variability. (b) The uranyl region of Raman spectra collected for ADU2 showing some differences in peak center. (c) The high-energy region of the Raman spectra of ADU2, showing differences in the number and intensity of peaks.

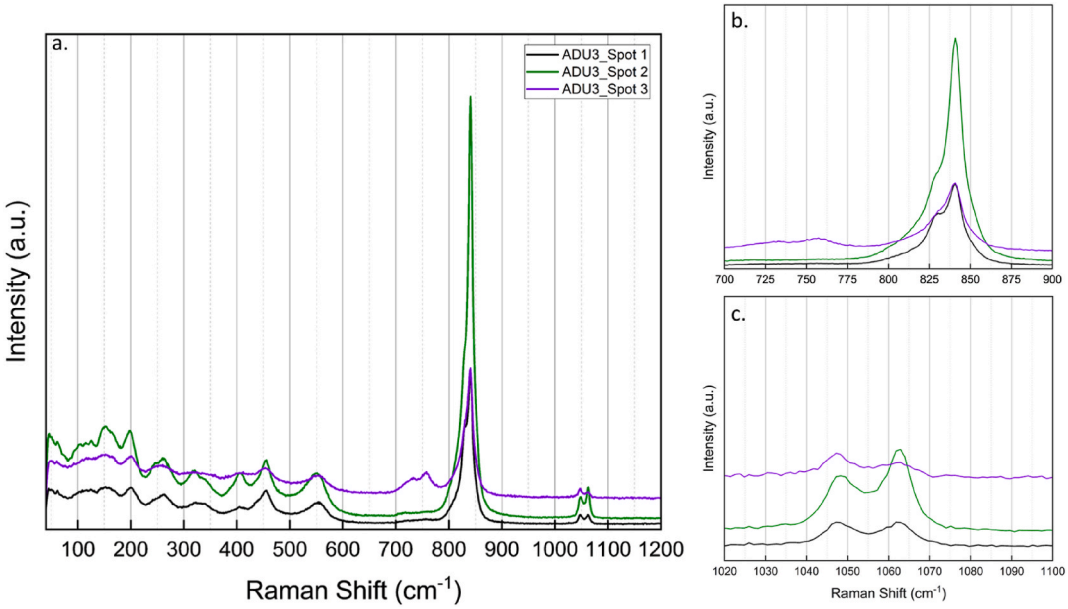


**Fig. 3.** (a) Raman spectra collected for three spots on the ADU3 sample show significant variability. (b) The uranyl region of Raman spectra collected for ADU3 displays differences in resolution of the $UO_2^{2+}$ symmetric stretching vibrational mode. (c) The high-energy region of the Raman spectra of ADU3 showing variability in intensity and resolution of peaks in this area.

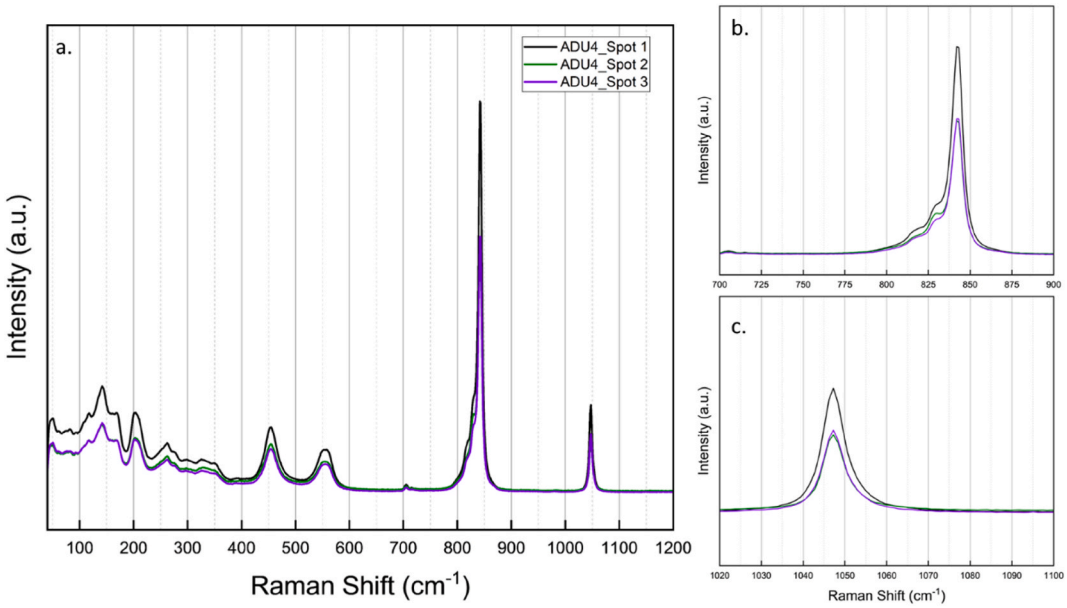


**Fig. 4.** (a) Raman spectra collected for three spots on the ADU4 sample to examine intrasample variability are fairly consistent across all datasets. (b) The uranyl region of Raman spectra collected for ADU4 showing only intensity differences. (c) The high-energy region of the Raman spectra of ADU4 displays consistent spectral features.

characterized by a doublet of peaks at approximately 1350 and 1375 $cm^{-1}$, and two other poorly resolved bands are seen at 1430 and 1650 $cm^{-1}$. Each of the three spectra for the ADU3 sample in the range of 1200–1800 $cm^{-1}$ show distinct spectral features. One spectrum has a lack of noteworthy spectroscopic features. An additional spectrum for this sample shows only broad peaks centered at approximately 1310 and 1600 $cm^{-1}$. The third dataset examined for ADU3 shows several broad low-intensity peaks centered at approximately 1,350, 1,370, 1,435, and 1665 $cm^{-1}$. Like we observed in the spectra collected for ADU4 in the range of 35–1200 $cm^{-1}$, at higher energy, datasets are consistent with regard to apparent spectroscopic features. The most intense peak in this region is centered at approximately 1340 $cm^{-1}$ and is accompanied by two lower intensity peaks at slightly higher energy, centered at

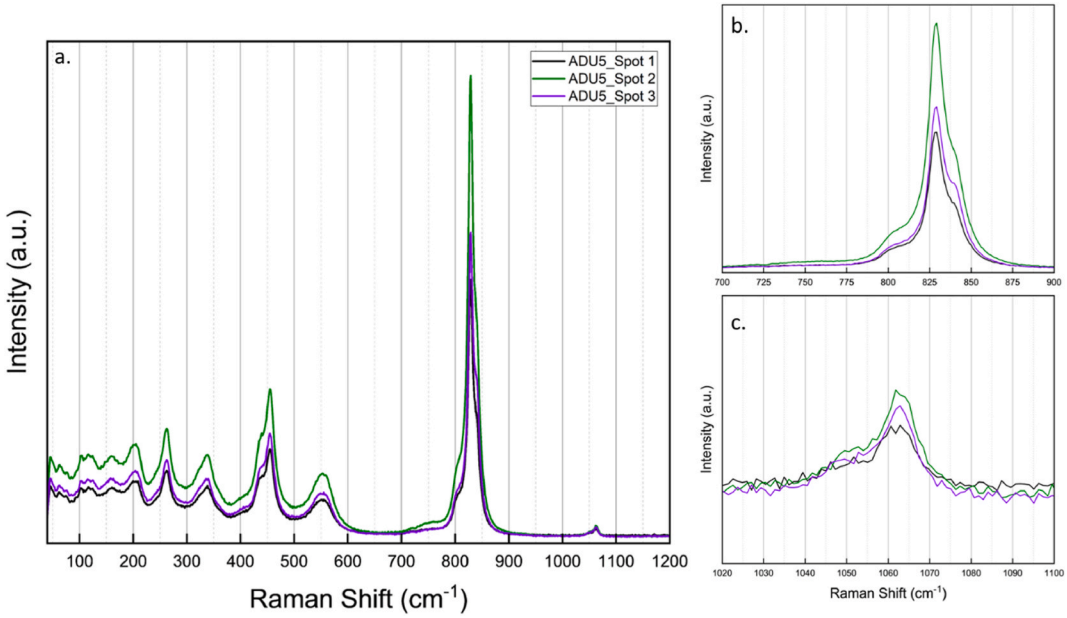


**Fig. 5.** (a) Raman spectra collected for three spots on the ADU5 sample showing limited intrasample variability. (b) The uranyl region of Raman spectra collected for ADU5 showing high- and low-energy shoulder features associated with the main uranyl band. (c) The high-energy region of the Raman spectra of ADU5.

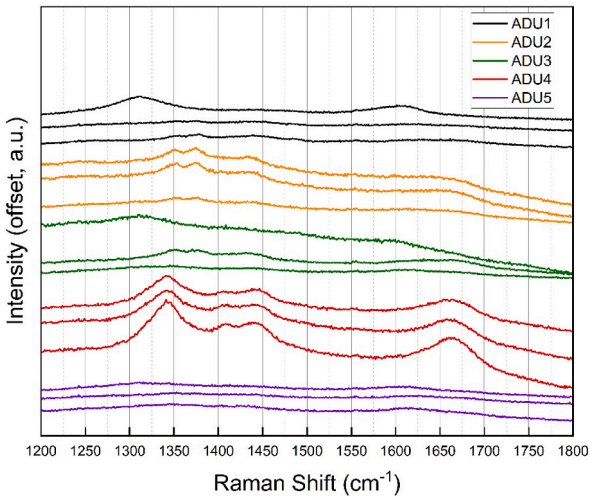


**Fig. 6.** Raman spectra collected for ADU samples in the range of 1200–1800 $cm^{-1}$. Significant intrasample variability is observed in the ADU2 and ADU3 samples, with the remainder of the ADU samples showing limited intrasample variability in this region. Three spectra for each sample were collected in this region, and datasets are offset for clarity.

approximately 1405 and 1445 $cm^{-1}$. An additional peak is seen in all spectra at approximately 1665 $cm^{-1}$. ADU5 are also consistent between 1200 and 1800 $cm^{-1}$, with limited spectral features seen in this region for all three spectra collected.

To summarize, ADU1, ADU4, and ADU5 are fairly consistent for intrasample spectra collected between 35 and 1200 $cm^{-1}$. These three materials exhibit constant spectral features, with the largest variability originating from differences in observed intensity. Conversely, the ADU2 and ADU3 ADU samples are heterogeneous in these regions, as indicated by the significant differences in spectroscopic features seen across multiple datasets collected for each sample. In the range of 1025–1075 $cm^{-1}$, both ADU2 and ADU3 show variability in the number and relative intensity of apparent vibrational modes in this region, and the potential origins will be discussed in a later section.

Examination of the higher energy region of the spectra, between 1200 and 1800 $cm^{-1}$ shows that the ADU1 indeed possesses intrasample variability, which we were not able to observe in the lower energy region of the spectra. While ADU2 appeared

**Table 2**
Raman and IR assignments for ADU spectra.

| Peak Center ($cm^{-1}$) | Assignment | Species | Samples | Activity (R=Raman, IR = infrared) |
|---|---|---|---|---|
| 203–290 | $UO_2^{2+}$ bending | metaschoepite | All | R |
| 320 | U-$O_{eq}$ | | ADU1, ADU2, ADU3 | R |
| 405 | U-$O_{eq}$ | metaschoepite | ADU1, ADU2, ADU3 | R |
| 435 | ? | | ADU5 | R |
| 450 | ? | | All | IR |
| 455 | O and U-O-H bending | metaschoepite | All | R |
| 545 | $H_2O$ | | ADU2 | R |
| 550 | $H_2O$ | | ADU1, ADU3, ADU5 | R |
| 550 | ? | | ADU4, ADU5 | IR |
| 555 | $H_2O$ | | ADU4 | R |
| 840 | $\nu_1$ $UO_2^{2+}$ | metaschoepite | ADU1, ADU2, ADU3, ADU4 | R |
| 900 | $\nu_3$ $UO_2^{2+}$ | | All | IR |
| 1045 | $\nu_1$ $NO_3^-$ | | ADU2, ADU3, ADU4, ADU5 | R |
| 1060 | $\nu_1$ $NO_3^-$ | | ADU1, ADU2, ADU3, ADU5 | R |
| 1350 | ? | | ADU2, ADU3, ADU4, ADU5 | R |
| 1350 | O-H bending | | ADU1, ADU2 | IR |
| 1375 | ? | | ADU2 | R |
| 1375 | O-H bending | | ADU1, ADU2 | IR |
| 1405 | $NH_4^+$ scissoring | | ADU4 | R |
| 1420 | $NH_4^+$ bending | | All | IR |
| 1430 | $NH_4^+$ scissoring | | ADU2, ADU3, ADU4, ADU5 | R |
| 1440 | $NH_4^+$ scissoring | | ADU1 | R |
| 1450 | ? | | ADU4 | R |
| 1555 | O-H scissoring | | All | R |
| 1610 | O-H scissoring | metaschoepite | ADU1, ADU3, ADU5 | R |
| 1620 | O-H bending | | All | IR |
| 1660 | O-H scissoring | | ADU4, ADU5 | R |

heterogeneous based on spectra in the range of 35–1200 $cm^{-1}$, this material appears homogeneous in the range of 1200–1800 $cm^{-1}$. At both high- and low-energy regions, distinct spectroscopic features are observed in each dataset collected for ADU3. Conversely, ADU4 and ADU5 spectra are consistent in all regions examined.

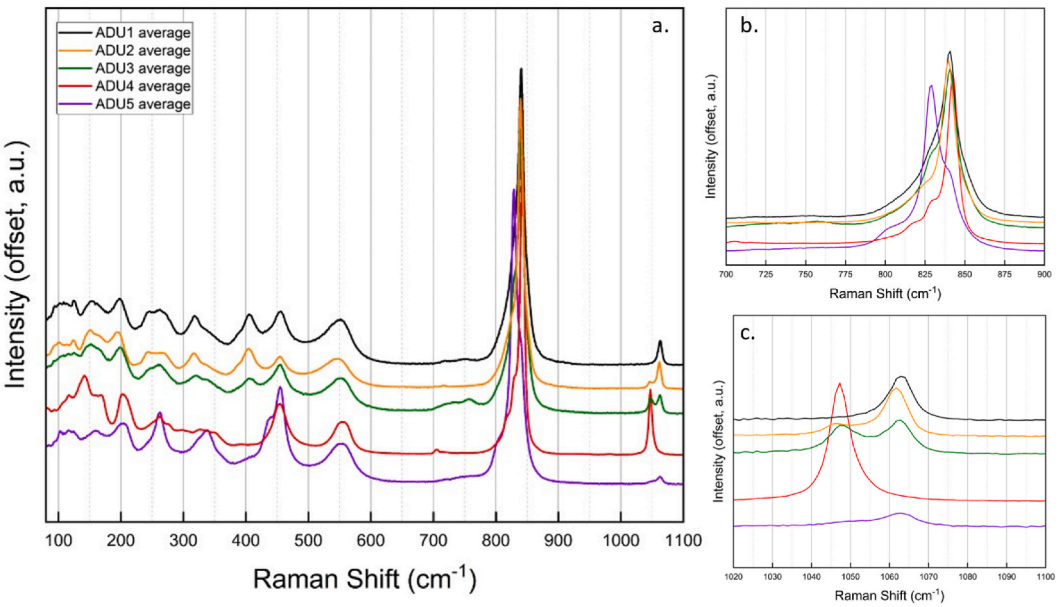


**Fig. 7.** (a) Average Raman spectra collected for all ADU samples to examine intersample variability, offset for clarity. (b) The uranyl region of average Raman spectra collected for ADU samples showing variability in peak center, shoulder modes, and band resolution. (c) The high-energy region of the Raman spectra of ADU samples illustrating differences in the number and intensity of peaks.

## 4. Discussion

### 4.1. Intersample variability: uranyl vibrational mode

Average Raman spectra (calculated from three spectra collected for each sample) for the five samples of ADU are shown in Fig. 7a, in which we observe significant intersample variability. The most apparent difference between sample spectra is visible in the uranyl region (Fig. 7b). In all spectra besides that of ADU5, a prominent peak is centered at approximately 840 $cm^{-1}$. Closer examination of this band in the ADU1, ADU2, ADU3, and ADU4 samples reveals additional complexity. The ADU3 and ADU1 sample spectra are centered right at 840 $cm^{-1}$; the ADU4 and ADU2 spectra are, however, shifted to a slightly higher or lower energy, with the main peak intensities centered at 842 and 839 $cm^{-1}$, respectively. Several low-energy shoulder modes are present for the ADU2, ADU3, and ADU4 samples. Observed asymmetry of the uranyl peak in the ADU1 sample indicates that similar, but poorly resolved, low-energy shoulder bands are also present. Interestingly, the position of some of the low-energy shoulder bands associated with uranyl vibrational modes appear to overlap with the highest intensity uranyl peak of the ADU5 sample. The ADU5 sample likewise possesses both high- and low-energy shoulder features in addition to the prominent uranyl band centered at approximately 828 $cm^{-1}$. The low-energy shoulder is located at approximately 800 $cm^{-1}$, whereas the high-energy feature appears at 840 $cm^{-1}$, likely originating from the same chemical coordination environment or species responsible for the most prominent uranyl peak in ADU2-3 and ADU1 samples.

The variability in reaction products among the ADU samples described in the PXRD section is echoed in our observations of the uranyl mode (Fig. 7b). The peak seen at 840 $cm^{-1}$ in all samples (with varying intensity) is likely attributable to the uranyl mode associated with the uranyl oxyhydroxide hydrate mineral metaschoepite, and from PXRD, this phase is indeed present in all ADU samples except for ADU5 [29,30]. The presence of uranyl oxyhydroxide hydrate phases within ADU samples is not surprising. Previous works involving PCA described similarities in the Raman spectra of ADU and uranyl hydroxide phases [20]. Likewise, Turcanu and Deju proposed that all compounds precipitated following standard ADU procedures result in formation of uranyl hydroxide (metaschoepite-like) phases [31]. While the exact mechanisms of preferential uranyl hydroxide formation are not elucidated by this work, we pose hypotheses in a later section that may guide future studies to investigate this.

The numerous shoulder peaks present in the uranyl region also allude to multiple U–O bond lengths and resultingly suggest that a variety of U coordination environments beyond the hexagonal bipyramidal units in metaschoepite are present. Bartlett and Cooney [32] present a correlation between the Raman frequency of the uranyl mode, and the corresponding U–O bond length from which that vibration originates. From applying the formula of Bartlett and Cooney to the position of the peak observed at 840 $cm^{-1}$, we see that bond lengths of 1.77 Å are likely present in the solid-phase sample. This is in excellent agreement with the $U–O_{yl}$ bond lengths observed in metaschoepite [24]. Slightly longer $U–O_{yl}$ bonds (1.78–1.8 Å) would produce the peaks observed at 828, 815, and 800 $cm^{-1}$. Despite the evidence suggesting that metaschoepite or related uranyl hydroxide phases are the primary solid-phase products of ADU precipitation, we see evidence of ammonium in the solid state, which will be described later.

### 4.2. Intersample variability: low-energy region

Variability in the low-energy region (Fig. 7a) of the Raman spectra of ADU is observed and likely arises from differences in secondary phases that precipitate in addition to metaschoepite/uranyl hydroxide, and perhaps from differences in the hydration state of the uranyl oxyhydroxyhydrate (metaschoepite) itself. Generally speaking, vibrational modes in the low-energy region of Raman spectra collected for uranyl oxysalt phases are associated with vibrations of equatorial oxygen atoms about uranium centers and in-plane scissoring (δ) modes associated with the $UO_2^{2+}$ unit [22,29,33]. Therefore, by examining this region of the spectra, we gain insight into the variability of linkages between individual U coordination polyhedra resulting from differences in polymerization of these units. Up to approximately 185 $cm^{-1}$, the ADU1, ADU2, ADU3, and ADU5 samples show similar spectroscopic features, with a diffuse group of peaks between approximately 85 and 135 $cm^{-1}$, and a broad feature centered at approximately 155 $cm^{-1}$. In the same region, the most intense peak of the ADU4 sample is located at approximately 142 $cm^{-1}$, which is accompanied both high- and low-energy shoulder peaks. All datasets possess a peak in the range of 180–225 $cm^{-1}$, although the center of this feature varies significantly among samples. Similarly, all spectra show multiple peaks between approximately 230 and 290 $cm^{-1}$, with differences in band intensity and resolution. Using density functional theory, Colmenero et al. [22] assign these bands to $\delta UO_2^{2+}$ scissoring vibrations. The variability (in both number and intensity of apparent vibrational modes) we observe between approximately 230 and 290 $cm^{-1}$ may subsequently originate from differences in the connectivity (e.g. hydrogen bonding) of axial oxygen atoms coordinating uranyl units because slight differences in bond strength would likely affect bond rigidity and resulting δ motions [34,35].

More pronounced differences between ADU samples are seen between approximately 290 and 600 $cm^{-1}$. First, we see a peak centered at approximately 320 $cm^{-1}$ in the ADU2, ADU3, and ADU1 samples, which likely originates from variations in uranium–oxygen equatorial bond lengths present in ADU precipitates [22]. Second, at 405 $cm^{-1}$, the ADU1, ADU2, and ADU3 samples show a peak that is likely also related to uranium–oxygen equatorial vibrational modes in metaschoepite [22,29] because from our PXRD results, these samples possess significant phase contributions from metaschoepite. The ADU4 and ADU5 samples do not possess a peak at 405 $cm^{-1}$, which may be due to the larger contributions of mixed-phase uranyl–ammonia/ammonium oxyhydrate phase contributions seen in PXRD. Third, all samples possess a peak at approximately 455 $cm^{-1}$, but the ADU5 sample also has a low-energy shoulder at approximately 435 $cm^{-1}$. Colmenero et al. suggest that bands in this region are attributable to combination bands of δ modes associated with equatorial O and U–O–H vibrations of metaschoepite [22]. The origin of the 435 $cm^{-1}$ shoulder band in ADU5 is not likely related to the presence of secondary phases, as all phase contributions observed in the PXRD data for this sample are present in other precipitates. It is worth noting however, that ADU5 was produced with the fastest stir rate of any ADUs investigated in this

work. We hypothesize that perhaps this feature originates from a unique structural attribute associated with this production parameter (e.g., grain boundary scattering) caused by small crystallite domains [36] resulting from rapid stirring/precipitation, and indeed we see only poorly defined crystallites in scanning electron microscopy images of ADU4 (Fig. S3). The final variable feature we observe in ADU spectra between approximately 290 and 600 $cm^{-1}$ is a band centered at 545–555 $cm^{-1}$. The center of this peak is variable across samples, with the ADU1, ADU3, and ADU5 sample coinciding with a center of 550 $cm^{-1}$. Conversely, this peak in the ADU2 sample is centered at approximately 545 $cm^{-1}$ and is located at 555 $cm^{-1}$ in ADU4. In metaschoepite, bands in this region are associated with $H_2O$-related vibrational modes, further suggesting variability in hydration state and hydrogen bonding within ADU precipitates.

### 4.3. Intersample variability: 1025–1075 $cm^{-1}$ region

Significant variability among ADU samples is observed in the range of 1025–1075 $cm^{-1}$ (Fig. 7c). The ADU2, ADU3, and ADU5 samples all display at least two apparent vibrational modes of varying relative intensity centered at approximately 1045 and 1060 $cm^{-1}$. Conversely, the ADU1 and ADU4 samples show only one peak in this region.

Bands in this region of uranyl compounds are typically associated with nitrate modes [37,38]. Despite PXRD results indicating that only sample ADU2 possesses nitrate, in the chemical form ammonium uranyl nitrate hydrate [27], our Raman results strongly suggest that there is indeed nitrate present in all samples. Consequently, we suppose that the variability in the number and intensity of vibrational modes in the range of 1025–1075 $cm^{-1}$ relates to the number of crystallographically distinct nitrate sites and the overall phase contributions of a nitrate-possessing material to the bulk ADU precipitate. For example, ADU4 likely only possesses one crystallographically unique nitrate mode based on the single intense peak centered at 1045 $cm^{-1}$, but some constituent of the ADU2 sample probably has at least two unique nitrate groups. While ammonium uranyl nitrate hydrate does not have a published crystal structure, its anhydrous counterpart does and possesses multiple crystallographically distinct nitrate sites, which agrees with the multiple nitrate modes seen in Fig. 7C.

The presence of some nitrate-rich uranyl phases in the mixed phase precipitates that result from ADU processes is probable because aqueous uranyl nitrate is a precursor to ADU. Likewise, the absence of nitrate-rich phases in our PXRD data does not definitively indicate that $NO_3^{2-}$ is not present since phase fractions less than approximately 5 wt % are typically not detectable using this technique. All ADU samples possess contributions from a phase best described in the PDF as $2UO_3{\cdot}NH_3{\cdot}3H_2O$ or $UO_3{\cdot}NH_3{\cdot}H_2O$ (see Results), which correspond to materials observed by Cordfunke [4] and Debets and Loopstra [5]. The materials $2UO_3{\cdot}NH_3{\cdot}3H_2O$ or $UO_3{\cdot}NH_3{\cdot}H_2O$ were initially prepared by reaction of $UO_3$, water, and ammonia, likely resulting in this proposed stoichiometry. However, these authors do not provide a crystal structure solution, and other works have observed formation of this phase in the presence of uranyl nitrate and ammonium hydroxide [26]. Because the exact structural details of $2UO_3{\cdot}NH_3{\cdot}3H_2O$ and $UO_3{\cdot}NH_3{\cdot}H_2O$ remain unknown, we hypothesize that these indeed may contain nitrate based on our Raman results.

### 4.4. Inter- and intrasample variability: 1200–1800 $cm^{-1}$ region

Average spectra of Raman datasets collected for ADU samples in the range of 1200–1800 $cm^{-1}$ are shown in Fig. 8 and exhibit significant variability. Although all datasets display a broad band of several spectroscopic features between approximately 1250 and 1500 $cm^{-1}$, several distinct peaks are seen. The ADU1 sample shows several diffuse bands between 1300 and 1400 $cm^{-1}$ and one more clearly defined peak centered at approximately 1440 $cm^{-1}$. The ADU2 sample is characterized by two fairly well resolved peaks at 1350 and 1375 $cm^{-1}$, and a broader, lower intensity band at approximately 1430 $cm^{-1}$. The ADU3, ADU4, and ADU5 samples all have

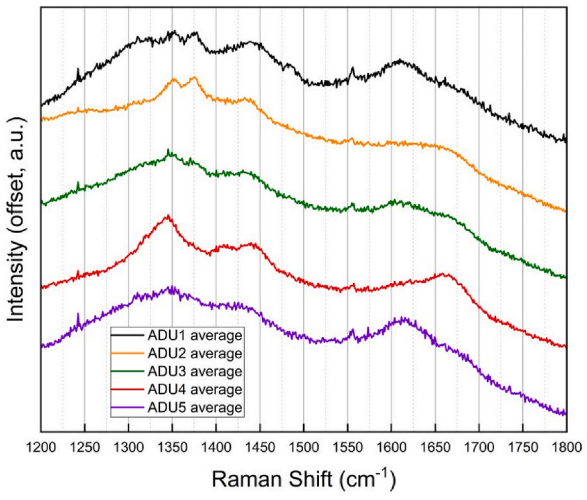


**Fig. 8.** Average Raman spectra collected for ADU samples in the range of 1200–1800 $cm^{-1}$ (offset for clarity) show distinct spectroscopic features that may be correlated with production route.

a peak centered at approximately 1350 $cm^{-1}$, which is similar to what we observe for the ADU2 sample; however, the second peak (1375 $cm^{-1}$) in ADU2 is not visible in the ADU4 and ADU5 samples. ADU3, ADU4, and ADU5 also all possess a broad feature at approximately 1430 $cm^{-1}$, again similar to ADU2, but the ADU4 sample appears to have a more clearly resolved band at 1350 $cm^{-1}$ relative to other samples. The ADU4 sample shows two distinct peaks (centered at 1405 and 1450 $cm^{-1}$) contributing to the broad intensity between 1400 and 1450 $cm^{-1}$. Variability in the number of and nature of connectivity of $NH_4^+$ moieties between ADU samples may be a contributor to the spectroscopic variances in the range of approximately 1250–1500 $cm^{-1}$ as $NH_4^+$ scissoring modes are reported in the range of 1430–1390 $cm^{-1}$ within crystalline solids [39]. Raman assignments provided by Colmenero et al. [22] and Ho Mer Lin et al. [21] also indicate that variability in this region originates from phase components beyond the uranyl hydroxide or metaschoepite phases. Colmenero et al. do not predict any Raman active modes in the range of approximately 1250–1500 $cm^{-1}$ for metaschoepite, and Ho Mer Lin et al. do not observe any prominent vibrational modes in experimental spectra presented for uranyl hydroxide, further implying that spectroscopic features in this region are attributable to the presence of $NH_4^+$ moieties.

All spectra collected for ADU show a peak centered at approximately 1555 $cm^{-1}$, although the origin of this mode remains unclear. We can assign additional features between 1575 and 1700 $cm^{-1}$ to oxygen–hydrogen scissoring modes of $H_2O$, however. The ADU1, ADU3, and ADU5 samples all show a band centered at 1610 $cm^{-1}$, which is in excellent agreement with the location of the oxygen–hydrogen band predicted by Colmenero et al. for metaschoepite. Unsurprisingly, our PXRD data also show that metaschoepite contributes significantly to the powder diffractograms of these samples. We also identified a significant phase contribution of metaschoepite to the ADU2 sample, but based on the absence of the oxygen–hydrogen band in the Raman spectrum of this phase, ADU2 may have undergone surface dehydration as the dehydration and rehydration of uranyl oxyhydroxyhydrate phases like metaschoepite has been reported in the literature [40]. ADU4 and ADU5 show a peak at approximately 1660 $cm^{-1}$, and this higher energy mode may be attributable still to oxygen–hydrogen vibrations, albeit in a different structural configuration relative to samples with large phase contributions of metaschoepite.

### 4.5. *Intersample variability: ADU IR spectra*

ATR-IR spectra collected for ADU are complex (Fig. 9) but are broadly in good agreement with the limited IR spectra for ADU available in the literature. Where possible, we use data provided by Sato and Shiota [14] to assign spectroscopic features in our ATR-IR spectra. All datasets show an intense band located at approximately 450 $cm^{-1}$, a low-intensity band at 670 $cm^{-1}$, and the ADU4 and ADU5 samples possess an additional low-intensity feature at 550 $cm^{-1}$. The ADU4 and ADU5 samples also display an apparent triplet of modes between approximately 720 and 830 $cm^{-1}$. The $\nu_3$ antisymmetric stretching vibration associated with the uranyl unit is seen at approximately 900 $cm^{-1}$ for all samples [14,41]. All $\nu_3$ bands show significant asymmetry, indicating the presence of multiple unique uranyl sites [42]. The $\nu_3$ bands of the ADU4 and ADU5 samples, in particular, possess significant contributions from shoulder modes.

Intense absorption features are observed for all samples between 1250 and 1500 $cm^{-1}$. The ADU3, ADU4, and ADU5 samples have a doublet of bands at 1315 and 1340 $cm^{-1}$, which are likely attributable to oxygen–hydrogen bending vibrations [43]. The ADU1 and ADU2 samples also have bands in this region, albeit shifted to approximately 1350 and 1375 $cm^{-1}$, which could indicate slight differences in oxygen–hydrogen connectivity in these samples relative to the ORNL 2, 3, and 4 samples. All ADU samples possess absorption bands centered at approximately 1420 $cm^{-1}$, with varying degrees of asymmetry and intensity. The most intense absorption here is seen in the ADU4 sample, but the occurrence of this feature in all samples indicates that $NH_4^+$ is indeed present in all materials, as this band is assigned to bending vibrations of $NH_4^+$ [14,43]. Additional, low-intensity oxygen–hydrogen bending vibrations are seen in all samples at approximately 1620 $cm^{-1}$ [14,43].

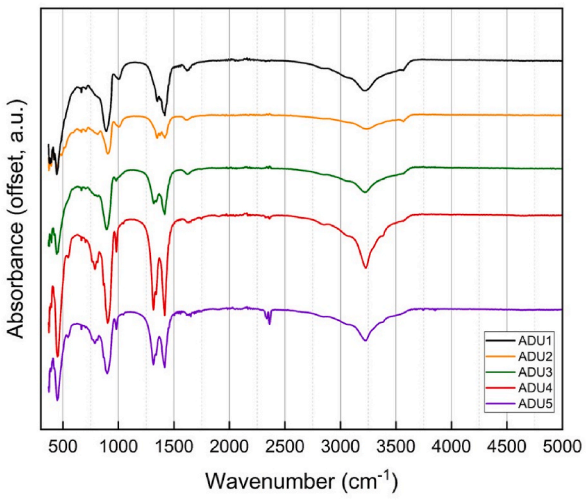


**Fig. 9.** IR spectra collected for samples of ADU, offset for clarity.

The intense absorption multiplet seen in our samples, centered at approximately 3230 $cm^{-1}$ likely originates from a combination of oxygen–hydrogen and $NH_4^+$ stretching vibrations, based upon assignments from Sato and Shiota [14]. Closer examination of these bands reveals distinct peaks at approximately 3385 $cm^{-1}$ in the ADU4 and ADU5 samples; interestingly, these samples were produced with a different stir rate during ammonia addition relative to the remaining samples. Further spectroscopic indicators of production parameters, in particular, differences in the solid phase ADU4 and ADU5 samples, based on results from principal component analysis of Raman spectra will be discussed in the next section.

### 4.6. Intersample variability: PCA and process variables

To explore the possibility that process variables related to ADU production are contributing to differences in subtle spectroscopic features, we conducted PCA of Raman spectra. First, the full spectra in the range of 35–1200 $cm^{-1}$ for all Raman datasets collected for ADU samples were subjected to a 0,1-normalization method to ensure that variations in absolute intensity would not influence overall PCA results. Then, using the OriginPro software suite, initial principal components were determined using a built-in algorithm. Upon examining the scree plot generated from PCA, four components were then used for calculation. The first four principal components account for 98.93 % of variability among spectra. Principal component spectra (loading plots) for each of these four components are shown in Fig. S9 in the Supporting Information. We discuss each of the principal component spectra before examining the coefficients of each principal component as a means of understanding real physicochemical indicators that contribute to separation based on PC scores seen in Fig. 10.

PC1 spectra are characterized by a high-intensity peak centered at 840 $cm^{-1}$ with a low-energy shoulder peak associated with it. Again, this spectrum is similar to that of the uranyl oxyhydroxyhydrate mineral metaschoepite. Broad, low-intensity features are located between approximately 700 and 775 $cm^{-1}$. The range between approximately 40 and 600 $cm^{-1}$ shows a complex convolution of vibrational modes, with at least 10 peaks contributing to observed intensity. Notably, at high energy, two peaks are present between 1040 and 1075 $cm^{-1}$, with the lower energy peak at 1045 $cm^{-1}$ possessing slightly higher intensity than the peak at 1060 $cm^{-1}$. PC1 accounts for 90.56 % of variance among samples; most of the spectroscopic information we see in this PC is no different than what is easily examined by qualitative analysis of sample spectra further indicating that metaschoepite is the primary phase that results from ADU precipitation.

PC2, unlike PC1, contains more subtle spectroscopic information, as this PC accounts for only 5.88 % of variability among sample spectra. Four peaks in the low-energy region, centered at 262, 337, 436, and 456 $cm^{-1}$ are seen. In PC2, we also observe a shift in the intensity of the prominent uranyl mode, with negative intensity at approximately 840 $cm^{-1}$, and positive intensity at 829 $cm^{-1}$. This shift indicates that samples with high scores along PC2 possess fewer spectroscopic features that are associated with metaschoepite. We also observe from PC2 spectra negative intensity at 1045 $cm^{-1}$.

The PC3 spectrum accounts for 4.88 % of variability among samples and shows several areas of positive intensity in the low-energy region, with subtle peaks visible at 140, 210, 453, and 560 $cm^{-1}$. Notably, this PC is characterized by a lower intensity within the uranyl region, with a significant band of negative intensity centered at 840 $cm^{-1}$. Two areas of positive intensity are seen flanking the 840 $cm^{-1}$ feature, centered at 829 and 845 $cm^{-1}$. PC3, unlike PC2, shows positive intensity at 1045 $cm^{-1}$.

The contributions of PC4 to overall spectroscopic variability are minor, as this component accounts for only 1.89 % of variability among samples. Nevertheless, we see the broad, low-intensity features that were observed in many individual sample spectra captured within this PC. The most prominent feature of the overall low-magnitude features in PC4 is an apparent doublet of peaks between 700 and 800 $cm^{-1}$. As a result, we expect to see high scores along PC4 for samples in which this feature was observed.

Plotting the coefficients of PC2 vs. PC1 (Fig. 10a) results in significant separation of sample spectra. ADU1, ADU2, ADU3, and ADU4 have PC1 coefficients between 0.250 and 0.275, meaning they are similar in terms of the contributions of features seen in PC1 to overall spectra. Likewise, these samples have similar negative contributions along PC2. The ADU5 sample has significantly higher PC2 contributions than the rest of the samples and significantly lower contributions along PC1. The ADU5 spectra, therefore, have much stronger contributions from a solid phase with a prominent uranyl vibrational mode at 830 $cm^{-1}$, rather than being dominated by spectra similar to metaschoepite based on our previous discussion of features in the PC spectra. Notably, the ADU5 sample was prepared with a solution stir rate much higher than the other samples, suggesting that this process variable induces the formation of a unique solid-phase material, as faster stir rates during production may perturb normal precipitation processes resulting in a different solid-phase product.

The slow stir rate used during the preparation of the ADU4 sample becomes evident upon examination of PC3 vs. PC1 (Fig. 10b). An approximately linear correlation between coefficients of PC1 and PC3 is observed for ADU1, ADU2, and ADU3 samples, which were all prepared with a stir rate of 400 rpm, further suggesting that the stir rate used during preparation significantly impacts the speciation of precipitated phases. ADU5 again is an outlier because of its lower coefficient of PC1. This sample was prepared with a stir rate of 500–600 rpm. Likewise, a slower stir rate of 100–130 rpm was used to prepare ADU4, which has a high contribution of PC3 relative to other samples and appears distinct from the 400 rpm samples (ADU1-3).

The high contribution of PC2 and PC3 to ADU5 and ADU4 samples, respectively, is further displayed in Fig. 10c, which shows components of PC2 vs. PC3. Again, clustering of the ADU1-3 is observed. Recalling our assessment of the principal component spectra, we can surmise that the high contributions of PC2 to ADU5 arise from low-intensity high-energy vibrational modes in the range of 1045–1060 $cm^{-1}$. Furthermore, these samples may be characterized by a redshift with respect to intensity of spectroscopic features in the uranyl region, and additional bands in the low-energy (~200–450 $cm^{-1}$) region of the spectra. The high contribution of PC3 to ADU4 is likely characterized by a redshift occurring in the 1045–1060 $cm^{-1}$ region of the spectrum and a shift in intensity within the uranyl region of spectra for these samples.

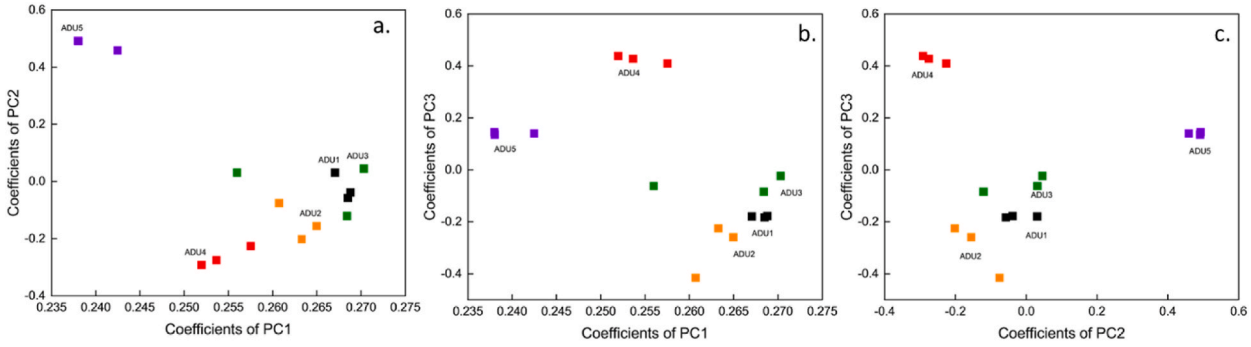


**Fig. 10.** Binary plots of scores along (a) PC1 and PC2, (b) PC1 and PC3, and (c) PC2 and PC3. Significant separation of ADU4 and ADU5 is observed and may be attributable to spectroscopic differences arising from variability in process parameters.

Although we cannot definitively assign spectroscopic features to production parameters using PCA alone, spectroscopic variability present in our samples does appear to correlate to differences in the stir rate used during synthesis. Notably, no influence on preparation temperatures used for ADU precipitation is observed in our PCA analysis. Aside from ADU1, which was prepared with a solution temperature of 60 °C, all remaining ADU samples were prepared at solution temperature of 20 °C. If subtle spectroscopic differences were to arise as a function of solution temperature, separation of ADU1 datapoints from the rest of the samples would likely be observed in our PCA results shown in Fig. 10. PCA of Raman data, combined with qualitative Raman and IR assignment based on the literature, and phase identification from PXRD indicate that significant differences in the obtained materials result from variability in ADU processing parameters. The overarching result of PCA analysis is further confirmation that the primary phase precipitated during ADU preparation is similar to the mineral phase metaschoepite, as indicated by the prominent spectral features in PC1 that are attributable to a metaschoepite-like phase.

## 5. Conclusions

Despite the widespread appearance of ADU in uranium processing, we confirm previous suggestions that significant variability in the solid-phase reaction products may be coupled to production variables. The higher temperature used to prepare ADU1, and the interruption during the synthesis of ADU2, appear to have less influence on the solid-phase identity than stir rate because of the spectroscopic similarity between ADU1, ADU2, and ADU3. The abundance of a metaschoepite-like phase, although observed previously, is correlated here with fast to intermediate stir rates, as evidenced by the lack of metaschoepite in the ADU4 sample, which was prepared with a stir rate of 100–130 rpm. One possible explanation for the abundance of metaschoepite-like phases in faster stir rates may be the relatively faster reaction kinetics of metaschoepite compared to other phases. Although we did not examine this possibility systematically, further studies could explore the precipitation kinetics of individual phases in more detail to further elucidate this mechanism.

Our Raman results indicate that nitrate is likely present in all samples, with varying local coordination suggested by the variable number and intensity of nitrate modes in the Raman spectra of these materials. Raman spectroscopy also shows that multiple uranyl coordination environments are present in all ADU samples, with the most prominent spectroscopic feature in the uranyl regions being the $\nu_1$ U–$O_{yl}$ symmetric stretching vibrational mode. In most samples, this appears at approximately 840 $cm^{-1}$, further evidencing the strong metaschoepite phase contributions to ADU. However, ADU5 is characterized by an additional peak at slightly lower energy (828 $cm^{-1}$), again suggesting that the faster stir rate used to prepare this sample (600–500 rpm) results in a metaschoepite-like phase, albeit with additional spectroscopic contributions that may be related to this fastest stir rate.

The spectroscopic details associated with differences in ADU precipitation are further echoed in our PCA results. Distinct separation of ADU4 and ADU5 are observed in Fig. 10, and the variables that are unique for these samples relative to the remainder are the stir rates used for preparation. Though we observed differences in the solid phases obtained from ADU precipitation using PXRD, a more granular understanding of the variability within individual samples was provided by examining multiple spectra collected for particles of each sample. Collecting Raman spectroscopic data in the range of 35–100 $cm^{-1}$ enabled identification of intrasample variability in some samples, but without our additional data collections in the range of 1200–1800 $cm^{-1}$, intrasample variability in the ADU1 sample would have been missed. Likewise, the complimentary Raman and IR spectroscopic datasets allowed for identification of both nitrate and ammonium vibrational modes in our samples.

The exact structural details of some phases of ammonium diuranate remain unknown, we provide here new insight into the structural and spectroscopic features in materials resulting from ADU precipitation as related to process parameters. We show that stir rate appears to be a stronger determinant of ultimate phase composition than precipitation temperature. We further provide high-quality PXRD data, and Raman, and IR spectra for ADU with known production parameters. With certainty, we can affirm previous literature reports that describe ADU as multiphase mixture rather than a discrete solid phase having the composition $NH_4U_2O_7$. Additional investigations of ADU with other processing parameters, as well as explorations of the hydrolysis and environmental aging of ADU may help to further clarify the exact details of this common fuel cycle material.

## CRediT authorship contribution statement

**Tyler L. Spano:** Writing – original draft, Visualization, Methodology, Investigation, Formal analysis, Conceptualization. **Caleb Redding:** Writing – review & editing, Resources. **Jordan M. Roach:** Writing – review & editing, Investigation, Formal analysis. **Cody A. Nizinski:** Writing – review & editing, Resources. **Evan Warzecha:** Writing – review & editing, Resources. **Matthew Athon:** Writing – review & editing, Resources. **Rodney Hunt:** Resources. **Andrew Miskowiec:** Writing – review & editing, Supervision, Resources, Investigation. **Jennifer Ladd-Lively:** Writing – review & editing, Project administration, Funding acquisition.

## Data availability

Data will be made available on request.

## Declaration of competing interest

The authors declare the following financial interests/personal relationships which may be considered as potential competing interests:Tyler L. Spano reports financial support was provided by National Nuclear Security Administration. If there are other authors, they declare that they have no known competing financial interests or personal relationships that could have appeared to influence the work reported in this paper.

## Acknowledgments

The authors thank Dustin Summers and J. J. Quinn for their support. This manuscript was significantly improved by helpful discussions with Drs. Daniel Felton and Kathryn Peruski, and the comments of two anonymous reviewers. This work was funded by the Office of Defense Nuclear Nonproliferation Research and Development Forensics Program within the US Department of Energy's National Nuclear Security Administration.

## Appendix A. Supplementary data

Supplementary data to this article can be found online at https://doi.org/10.1016/j.heliyon.2025.e42568.

## References

[1] E.H.P. Cordfunke, Composition and structure of ammonium uranates, J. Inorg. Nucl. Chem. 32 (9) (1970) 3129–3131, https://doi.org/10.1016/0022-1902(70)80390-6.
[2] R.A. Ewing, A. Bearse, Investigation of Ammonium Uranates, Battelle Memorial Institute, Columbus, OH, 1956.
[3] S. Manna, C. Basak, U.R. Thakkar, S. Thakur, S.B. Roy, J.B. Joshi, Study on effect of process parameters and mixing on morphology of ammonium diuranate, J. Radioanal. Nucl. Chem. 310 (2016) 287–299, https://doi.org/10.1007/s10967-016-4883-5.
[4] E.H.P. Cordfunke, On the uranates of ammonium—I: the ternary system $NH_3$–$UO_3$–$H_2O$, J. Inorg. Nucl. Chem. 24 (3) (1962) 303–307, https://doi.org/10.1016/0022-1902(62)80184-5.
[5] P. Debets, B.O. Loopstra, On the uranates of ammonium—II: X-ray investigation of the compounds in the system $NH_3$–$UO_3$–$H_2O$, J. Inorg. Nucl. Chem. 25 (8) (1963) 945–953, https://doi.org/10.1016/0022-1902(63)80027-5.
[6] W. Stuart, T. Whateley, Composition and structure of ammonium uranates, J. Inorg. Nucl. Chem. 31 (6) (1969) 1639–1647, https://doi.org/10.1016/0022-1902(69)80378-7.
[7] S. El-Fekey, M. Khilla, N. Rofail, Thermal decomposition of ammonium uranate; X-ray study, Radiochim. Acta 37 (3) (1984) 153–158, https://doi.org/10.1524/ract.1984.37.3.153.
[8] B.N. Murty, P. Balakrishna, R. Yadav, C. Ganguly, C, Influence of temperature of precipitation on agglomeration and other powder characteristics of ammonium diuranate, Powder Technol. 115 (2) (2001) 167–183, https://doi.org/10.1016/S0032-5910(00)00336-3.
[9] S. Paik, S. Biswas, S. Bhattacharya, S. Roy, Effect of ammonium nitrate on precipitation of ammonium di-uranate (ADU) and its characteristics, J. Nucl. Mater. 440 (1–3) (2013) 34–38, https://doi.org/10.1016/j.jnucmat.2013.04.011.
[10] J. Janov, P.G. Alfredson, V. Vilkaitis, The influence of precipitation conditions on the properties of ammonium diuranate and uranium dioxide powders, J. Nucl. Mater. 44 (2) (1972) 161–174, https://doi.org/10.1016/0022-3115(72)90094-3.
[11] J. Woolfrey, The Effect of pH on the Properties of Ammonium Uranate Precipitated with Gaseous Ammonia, Australian Atomic Energy Commission Research Establishment, 1976.
[12] S.T. Heffernan, N.-C. Ly, B.J. Mower, C. Vachet, I.J. Schwerdt, T. Tasdizen, L.W. McDonald IV, Identifying surface morphological characteristics to differentiate between mixtures of $U_3O_8$ synthesized from ammonium diuranate and uranyl peroxide, Radiochim. Acta 108 (1) (2019) 29–36, https://doi.org/10.1515/ract-2019-3140.
[13] B. Lee, S. Yang, D. Kwak, H. Jo, Y. Lee, Y. Bae, J. Lee, Ammonium uranate hydrate wet reconversion process for the production of nuclear-grade $UO_2$ powder from uranyl nitrate hexahydrate solution, Nucl. Eng. Technol. 55 (6) (2023) 2206–2214, https://doi.org/10.1016/j.net.2023.02.019.
[14] T. Sato, S. Shiota, Thermal decomposition of ammonium uranates, J. Therm. Anal. 30 (1985) 107–120, https://doi.org/10.1016/j.net.2023.02.019.
[15] M. Said, S.N. Perry, S.E. Benjamin, A.E. Hixon, Formation of ammonium uranate on uranium dioxide during aging under controlled storage conditions, J. Nucl. Mater. 555 (2021) 153078, https://doi.org/10.1016/j.jnucmat.2021.153078.
[16] L.J. Bonales, N. Rodríguez-Villagra, I. Sánchez-García, O.R. Montoro, U(VI) speciation studies by Raman spectroscopy technique in the production of nuclear fuel, Prog. Nucl. Energy 145 (2022) 104122, https://doi.org/10.1016/j.pnucene.2022.104122.
[17] F. Pointurier, O. Marie, Identification of the chemical forms of uranium compounds in micrometer-size particles by means of micro-Raman spectrometry and scanning electron microscope, Spectrochim. Acta B 65 (9–10) (2010) 797–804, https://doi.org/10.1016/j.sab.2010.06.008.
[18] A. Berlizov, D. Ho, A. Nicholl, T. Fanghänel, K. Mayer, Assessing hand-held Raman spectrometer FirstDefender RM for nuclear safeguards applications, J. Radioanal. Nucl. Chem. 307 (2016) 285–295, https://doi.org/10.1007/s10967-015-4160-z.

[19] D.H.M. Lin, D. Manara, Z. Varga, A. Berlizov, T. Fanghänel, K. Mayer, Applicability of Raman spectroscopy as a tool in nuclear forensics for analysis of uranium ore concentrates, Radiochim. Acta 101 (12) (2013) 779–784, https://doi.org/10.1524/ract.2013.2110.
[20] D.H.M. Lin, A.E. Jones, J.Y. Goulermas, P. Turner, Z. Varga, L. Fongaro, T. Fanghänel, K. Mayer, Raman spectroscopy of uranium compounds and the use of multivariate analysis for visualization and classification, Forensic Sci. Int. 251 (2015) 61–68, https://doi.org/10.1016/j.forsciint.2015.03.002.
[21] D.H.M. Lin, D. Manara, P. Lindqvist-Reis, T. Fanghänel, K. Mayer, The use of different dispersive Raman spectrometers for the analysis of uranium compounds, Vib. Spectrosc. 73 (2014) 102–110, https://doi.org/10.1016/j.vibspec.2014.05.002.
[22] F. Colmenero, J. Cobos, V. Timón, Periodic density functional theory study of the structure, Raman spectrum, and mechanical properties of schoepite mineral, Inorg. Chem. 57 (8) (2018) 4470–4481, https://doi.org/10.1021/acs.inorgchem.8b00150.
[23] M. Wojdyr, Fityk: a general-purpose peak fitting program, J. Appl. Crystallogr. 43 (5–1) (2010) 1126–1128.
[24] W.T. Weller, M.E. Light, T. Gelbrich, Structure of uranium (VI) oxide dihydrate, $UO_3{\cdot}2H_2O$; synthetic meta-schoepite $(UO_2)_4O(OH)_6{\cdot}5H_2O$, Acta Crystallogr. B 56 (4) (2000) 577–583, https://doi.org/10.1107/s0108768199016559.
[25] S. Le Roux, A. Van Tets, A., the space group determination from a single crystal of a member of the ADU family on a reciprocal lattice explorer, J. Nucl. Mater. 119 (1) (1983) 110–115, https://doi.org/10.1016/0022-3115(82)90306-3.
[26] M.H. Lloyd, K. Bischoff, K. Peng, H.U. Nissen, R. Wessicken, Crystal habit and phase attribution of U(VI) oxides in a gelation process, J. Inorg. Nucl. Chem. 38 (6) (1976) 1141–1147, https://doi.org/10.1016/0022-1902(76)80237-0.
[27] K.J. Notz, P.A. Haas, Properties and thermal decomposition of the double salts of uranyl nitrate-ammonium nitrate, Thermochim. Acta 155 (1989) 283–295, https://doi.org/10.1016/0040-6031(89)87154-0.
[28] H. Dunn, X-Ray Diffraction Data for Some Uranium Compounds, Oak Ridge National Laboratory, Oak Ridge, TN, 1956.
[29] T.L. Spano, T.A. Olds, M. McDonnell, R. Smith, J.L. Niedziela, A. Miskowiec, R. Kapsimalis, A.E. Shields, CURIES: compendium of uranium Raman and infrared experimental spectra, Am. Mineral. 108 (12) (2023) 2219–2233, https://doi.org/10.2138/am-2022-8738.
[30] G. Lu, A.J. Haes, T.Z. Forbes, Detection and identification of solids, surfaces, and solutions of uranium using vibrational spectroscopy, Coord. Chem. Rev. 374 (2018) 314–344, https://doi.org/10.1016/j.ccr.2018.07.010.
[31] C. Turcanu, R. Deju, Thermal analysis of ammonium diuranate, Nucl. Technol. 45 (2) (1979) 188–192, https://doi.org/10.13182/NT79-A32310.
[32] J.R. Bartlett, R.P. Cooney, On the determination of uranium–oxygen bond lengths in dioxouranium (VI) compounds by Raman spectroscopy, J. Mol. Struct. 193 (1989) 295–300, https://doi.org/10.1016/0022-2860(89)80140-1.
[33] F. Colmenero, A.M. Fernández, J. Cobos, V. Timón, Periodic DFT study of the thermodynamic properties and stability of schoepite and metaschoepite mineral phases, ACS Earth Space Chem. 3 (1) (2019) 17–28, https://doi.org/10.1021/acsearthspacechem.8b00109.
[34] F.C. Hawthorne, The role of OH and $H_2O$ in oxide and oxysalt minerals, Z. Kristallogr. Cryst. Mater. 201 (1–4) (1992) 183–206, https://doi.org/10.1524/zkri.1992.201.3-4.183.
[35] F.C. Hawthorne, Toward theoretical mineralogy: a bond-topological approach, Am. Mineral. 100 (4) (2015) 696–713, https://doi.org/10.2138/am-2015-5114.
[36] T.L. Spano, A.E. Shields, J.L. Niedziela, A. Miskowiec, Unexpected features in the optical vibrational spectra of δ-$UO_3$, Front. Nucl. Eng. 1 (2022) 995292, https://doi.org/10.3389/fnuen.2022.995292.
[37] P. Khulbe, A. Agarwal, G. Raghuvanshi, H. Bist, H. Hashimoto, T. Kitagawa, T. Little, J. Durig, Raman studies of the vibrational dynamics and phase transitions in uranyl nitrate hexahydrate, J. Raman Spectrosc. 20 (5) (1989) 283–290, https://doi.org/10.1002/jrs.1250200503.
[38] K. Ohwada, Raman spectroscopic studies of some uranyl nitrate complexes, J. Coord. Chem. 8 (1) (1978) 35–39, https://doi.org/10.1080/00958977808073067.
[39] H. Baranska, A. Labudzinska, J. Terpinski, Laser Raman Spectrometry, Analytical applications, 1987.
[40] M.C. Kirkegaard, T.L. Spano, M.W. Ambrogio, J.L. Niedziela, A. Miskowiec, A.E. Shields, B.B. Anderson, Formation of a uranyl hydroxide hydrate via hydration of $[(UO_2F_2)(H_2O)]_7{\cdot}4H_2O$, Dalton Trans 48 (2019) 13685, https://doi.org/10.1039/C9DT02835H.
[41] G. Caldow, A. Van Cleave, R. Eager, The infrared spectra of some uranyl compounds, Can. J. Chem. 38 (6) (1960) 772–782, https://doi.org/10.1139/v60-112.
[42] E. Rabinowitch, R.L. Belford, Spectroscopy and Photochemistry of Uranyl Compounds: International Series of Monographs on Nuclear Energy, vol. 1, Elsevier, 2013.
[43] R.T. Conley, Infrared Spectroscopy, 1966.